Discrete element modelling of subglacial sediment deformation

Anders D. CHRISTENSEN[1], David L. EGHOLM[1], Jan A. PIOTROWSKI[1], and Slawek TULACZYK[2]

[1] Department of Geoscience, Aarhus University, Aarhus C, Denmark
[2] Department of Earth and Planetary Sciences, University of California, Santa Cruz, California, USA

Correspondence: `adc@geo.au.dk`, `http://cs.au.dk/~adc`

1. Introduction — Subglacial sediment in the glacial system

In glaciers, the gradient in the bed- and surface elevation is the primary control on the gravitationally driven ice flux from the accumulation zone towards the ablation zone. The equilibrium line altitude represents the climatically controlled borderline between higher regions of positive ice mass balance, and the lower altitudes where e.g. melting and calving cause a net ice mass loss (Cuffey and Paterson, 2010).

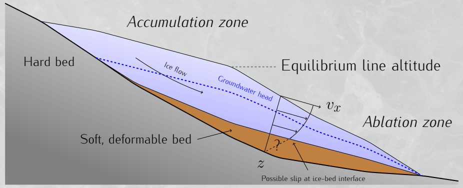

In addition to the viscous flow of the ice itself, the subglacial environment under a temperate glacier can contribute with two components to the movement of a glacier: 1) slip at the ice-bed interface caused by localized decoupling of the ice from the bed, or 2) deformation of subglacial sediment, which, if present, can contribute significantly to the overall motion of the system. Owing to the inaccessible nature of the subglacial environment, studies of subglacial sediment dynamics rely on sparse field data and laboratory experiments.

Ice sheet models that include subglacial deformation require an assumption regarding the rheology. Boulton and Hindmarsh (1987) suggested that subglacial sediment behaves like a viscoplastic material. Yet, laboratory experiments on subglacial material unambiguously demonstrate that it behaves plastically obeying the rate-independent Coulomb friction constitutive law (e.g. Kamb, 1991; Iverson and others, 1998; Tulaczyk and others, 2000). Schoof (2010) demonstrated a method for implementing the non-linear, Coulomb-frictional basal behavior in higher-order ice-sheet models.

We base our study on the fundamental observation that subglacial sediment is primarily a *granular material*, which is known to change rheological behavior depending on conditions such as the confining pressure, porosity and sediment grain velocities (e.g. Jaeger and others, 1996). Numerical simulations are designeded to mimic granular flow under subglacial stress and strain levels. This approach allows us to explore shear dynamics similar to what a glacier bed can be exposed to, and to simulate strain related structural signatures resembling those observed in real subglacial sediments.

2. Discrete Element Method

To simulate the granular material under subglacial conditions, a three-dimensional discrete element method (DEM) (Cundall and Strack, 1979) is employed. Through self-organizing complexity, the collective behavior of the discrete particles mirrors the dynamics of true granular materials.

The particles are treated as discrete, unbreakable, spherical units with their own mass (m) and inertia (I). The dynamics of the particle assemblage are examined under the influence of gravity and dynamic boundary conditions. Based on the net forces applied, the linear- ($\ddot{\mathbf{x}}$) and angular acceleration ($\dot{\omega}$) of each particle is calculated after each small time step, by application of Newton's law of motion for entities with constant mass:

$$m_i \ddot{\mathbf{x}}_i = \underbrace{m_i \mathbf{g} + \sum \left(\mathbf{f}^n_{ij} + \mathbf{f}^t_{ij} \right)}_{\text{Sum of forces on particle } i} \quad \text{and} \quad I_i \dot{\omega}_i = \underbrace{\sum \left(\mathbf{f}^t_{ij} \times \bar{R}_{ij} + T^r_{ij} \right)}_{\text{Sum of torques on particle } i}$$

Using the *soft-body contact model*, the particles are allowed to overlap, and the resulting contact forces are determined by the magnitude of the overlap, relative particle velocities, and the history of the contact.

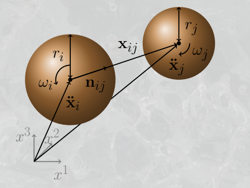

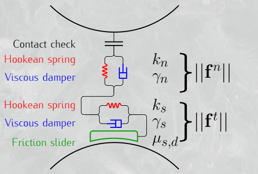

Contact criteria:
Overlap if: $\delta_{ij} = ||\mathbf{x}_{ij}|| - (r_i + r_j) < 0$

Normal force model:

$$\mathbf{f}^n_{ij} = \big(\underbrace{-k_n \delta_{ij}}_{\text{Linear-elastic repulsion}} \underbrace{-\gamma_n ||\dot{\delta}^n_{ij}||}_{\text{Viscous damping}}\big)\mathbf{n}_{ij}$$

Tangential force model:

$$\mathbf{f}^t_{ij} = \underbrace{-k_s \delta^t_{ij}}_{\text{Linear-elastic repulsion}} \underbrace{-\gamma_s \dot{\delta}^t_{ij}}_{\text{Viscous damping}}$$

The tangential shear force is limited by the Coulomb-friction criteria of static and dynamic friction:

$$||\mathbf{f}^t_{ij}|| \leq \underbrace{\mu_{s,d} ||\mathbf{f}^n_{ij}||}_{\text{Friction}}$$

The friction coefficient corresponds to static (μ_s) or dynamic (μ_d) values, dependent on the contact velocity.

3. CUDA implementation and visualization

The discrete-element algorithm is designed for graphics-processing unit (GPU) computation using the C/C++ CUDA API (NVIDIA, 2010a). Due to the parallel nature of the problem, the algorithm is able to utilize the high arithmetic potential of modern GPU's. Most components of the contact search-, contact model-, and integration routines are single-instruction, multiple-data problems, suited for the massively parallel structure of the GPU streaming multiprocessors (Kirk and Hwu, 2010; NVIDIA, 2010b). The neighbor search is reduced by discretizing the spatial model domain into a uniform, cubic grid with sorted cell lists, handled by the Thrust library. Simulation setup, control flow and data analysis is handled through a custom Python module.

Visualization of the particle assemblage is performed using a custom CUDA ray-tracing algorithm (Whitted, 1980; Christensen, 2011), which is memory-efficient by avoiding triangulation of the particle surfaces. The goal of the ray-tracing algorithm is to compute the shading of each pixel in the image. Creating a viewing ray from the eye into the scene, finding the closest intersection with a scene object, and computing the resulting color perform this. Benchmarks show a speedup of two magnitudes over an equivalent CPU implementation.

4. Simulation example

The spatial model domain consists of non-frictional upper- and lower walls, while the sides act as periodic boundaries. The following three steps are performed, with intermediate resetting of kinematic values:

1. **Gravitational consolidation**: A number of particles are initialized in a very loose packing at random, non-overlapping positions. The particles are allowed to settle under gravity.
2. **Consolidation under deviatoric normal stress**: The particles are consolidated under a fixed deviatoric stress (σ_0), applied by the dynamic top wall.
3. **Shearing**: The lowermost particles are fixed at their horizontal positions, while the uppermost particles are given a uniform, fixed, non-zero horizontal velocity. The shear stress is calculated as the sum of force components that the upper, fixed particles experience in the moving direction. The deviatoric stress of the upper wall is typically identical to the value during consolidation.

Here, an example simulation is presented with the following physical parameters:

Paramter	Symbol	Value
Particle count	N	10 000
Mean radius	$\bar{r}$	1×10^{-2} m
Material density	ρ	3.6×10^3 kg m^{-3}
Normal stiffness	k_n	1×10^9 N m^{-1}
Normal viscosity	γ_n	780 N s m^{-1}
Tangential stiffness	k_s	1×10^8 N m^{-1}
Tangential viscosity	γ_s	780 N s m^{-1}
Sliding friction coefficient (static)	μ_s	0.58
Sliding friction coefficient (dynamic)	μ_d	0.47
Rolling friction coefficient	μ_r	0.0
Computational time step	Δt	6.60×10^{-7} s
Deviatoric normal stress	σ_0	100×10^3 Pa
Shear strain rate	$\dot{\gamma}$	0.25 s^{-1}
Shear strain	γ	1

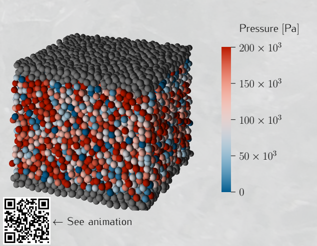

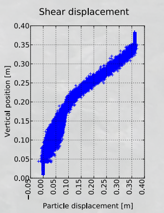

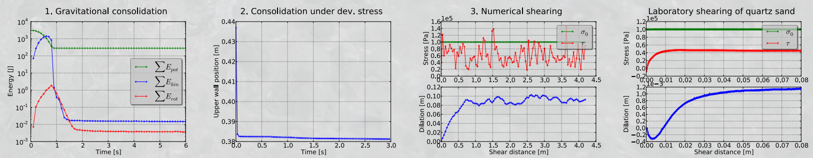

5. Conclusions

Numerically simulating granular dynamics under shearing motion can contribute with detailed insight into the internal material behavior under progressive shear strain, partly because of the high level of control of boundary conditions and physical parameters. Comparisons with physical experiments in a ring-shear apparatus demonstrate that the DEM implementation applied captures the true macroscopic stress dynamics of a granular material under subglacial shear.

Particle bonds will be implemented in the future, enabling experiments with fabric development under different states of the material. This topic is widely debated in the glacial geological community (e.g. Carr and Rose, 2003).

Implementing numerical simulation of porefluid flow is the logical next step because of the potential importance of melt-water pressure variations for subglacial sediment stability (e.g. Iverson, 2010). The porefluid solver will be based on a Lattice-Boltzmann type of model, which has already been demonstrated to perform well on GPUs.

The `sphere` DEM software package is licensed under the GNU Public License v. 3, and the project is maintained at `http://github.com/anders-dc/sphere`.

See also: Poster "**CUDA GPU-based full-Stokes finite difference modelling of glaciers**" by C.F. Brædstrup and D.L. Egholm, Thursday 17:30–19:00, XY-372.

Poster as PDF:

References

Boulton, G.S. and R.C.A. Hindmarsh, 1987. Sediment deformation beneath glaciers: rheology and geological consequences, *Journal of Geophysical Research*, **92**(B9), 9059–9082.

Carr, SJ and J. Rose, 2003. Till fabric patterns and significance: particle response to subglacial stress, *Quaternary Science Reviews*, **22**(14), 1415–1426.

Christensen, A.D., 2011. CUDA raytracing algorithm for visualizing discrete element model output, `http://users-cs.au.dk/adc/files/raytracer.pdf`.

Cuffey, K.M. and WSB Paterson, 2010. The physics of glaciers, *Elsevier, ed*, **4**, 693.

Cundall, P.A and O.D.L. Strack, 1979. A discrete numerical model for granular assemblies, *Géotechnique*, **29**, 47–65.

Iverson, N.R., 2010. Shear resistance and continuity of subglacial till: hydrology rules, *Journal of Glaciology*, **56**(200), 1104.

Iverson, N.R., T.S. Hooyer and R.W. Baker, 1998. Ring-shear studies of till deformation: Coulomb-plastic behavior and distributed strain in glacier beds, *Journal of Glaciology*, **148**, 634–642.

Jaeger, H.M., S.R. Nagel and R.P. Behringer, 1996. Granular solids, liquids, and gases, *Reviews of Modern Physics*, **68**(4), 1259–1273.

Kamb, B., 1991. Rheological nonlinearity and flow instability in the deforming bed mechanism of ice stream motion, *Journal of Geophysical Research*, **96**(B10), 16585–16.

Kirk, D.B. and W-M.W. Hwu, 2010. Programming Massively Parallel Processors, Morgan Kaufmann, Elsevier.

NVIDIA, 2010a. CUDA C Best Practices Guide Version, NVIDIA Corporation: Santa Clara, CA, USA, 3.2 ed., cA Patent 95,050.

NVIDIA, 2010b. CUDA C Programming Guide, NVIDIA Corporation: Santa Clara, CA, USA, 3.2 ed.

Schoof, C., 2010. Coulomb friction and other sliding laws in a higher order glacier flow model, *Math. Models. Meth. Appl. Sci*, **20**(1), 157–189.

Tulaczyk, S., W.B. Kamb and H.F. Engelhardt, 2000. Basal mechanics of ice stream B, West Antarctica 1. Till mechanics, *J. Geophys. Res*, **105**(B1), 463–481.

Whitted, T., 1980. An improved illumination model for shaded display, *Communications of the ACM*, **23**(6), 343–349.